J. Fluid Mech. (1998), *vol.* 358, *pp.* 335–356. Printed in the United Kingdom

Turbulent fountains in a stratified fluid

By LYNN J. BLOOMFIELD AND ROSS C. KERR

Research School of Earth Sciences, The Australian National University, Canberra, ACT 0200, Australia

(Received 4 October 1996 and in revised form 5 November 1997)

The turbulent fountain that results from the injection of a dense fluid upwards into a large tank of stably stratified fluid of lower density is studied experimentally and theoretically. For both axisymmetric and line fountains, we have used a combination of dimensional arguments and laboratory experiments to determine the initial height above the source at which the flow first comes to rest. Depending on the strength of the stratification and the fluxes of momentum and buoyancy at the source, the subsequent downflow may either spread along the base of the tank or intrude at an intermediate height in the environment. We determine both the height of intermediate intrusion and the critical condition for spreading along the base. We also relate numerical solutions of the entrainment equations to our experimental observations, and obtain effective entrainment coefficients for both axisymmetric and line fountains. Finally, we discuss the quantitative application of our results to the replenishment of magma chambers and to the heating or cooling of a room.

1. Introduction

The behaviour of turbulent jets, plumes and fountains has been explored theoretically and experimentally in a series of studies spanning the past forty years. Detailed reviews by Fischer *et al.* (1979), List (1982) and Turner (1986) outline how our current understanding has arisen from a combination of laboratory experiments, dimensional arguments and numerical solutions of the entrainment equations, which quantify the effects of the entrainment of surrounding fluid into the flow (Morton, Taylor & Turner 1956; Turner 1973).

The first study of a turbulent fountain in both homogeneous and stratified environments was by Morton (1959*a*). He used the entrainment equations to quantify the increasing radius and the decreasing buoyancy and velocity of dense fluid injected upwards into a lighter environment. However, these equations are only valid until the velocity of the first element of fluid in the flow is reduced to zero at the initial fountain height. To investigate the flow after the fluid reverses direction and falls around the central upflow, laboratory experiments are needed. Experiments in a homogeneous environment (Turner 1966; Campbell & Turner 1989; Baines, Turner & Campbell 1990) showed that the turbulent interaction between the up- and downflows restricts the rise of any further fluid and thus immediately reduces the initial fountain height to a smaller final value. This observed final height was related to the momentum and buoyancy fluxes at the source using dimensional arguments, and the relevant constants were found experimentally.

In this paper we investigate experimentally and theoretically the effect of an environmental density gradient on the behaviour of turbulent fountains. In § 2, we

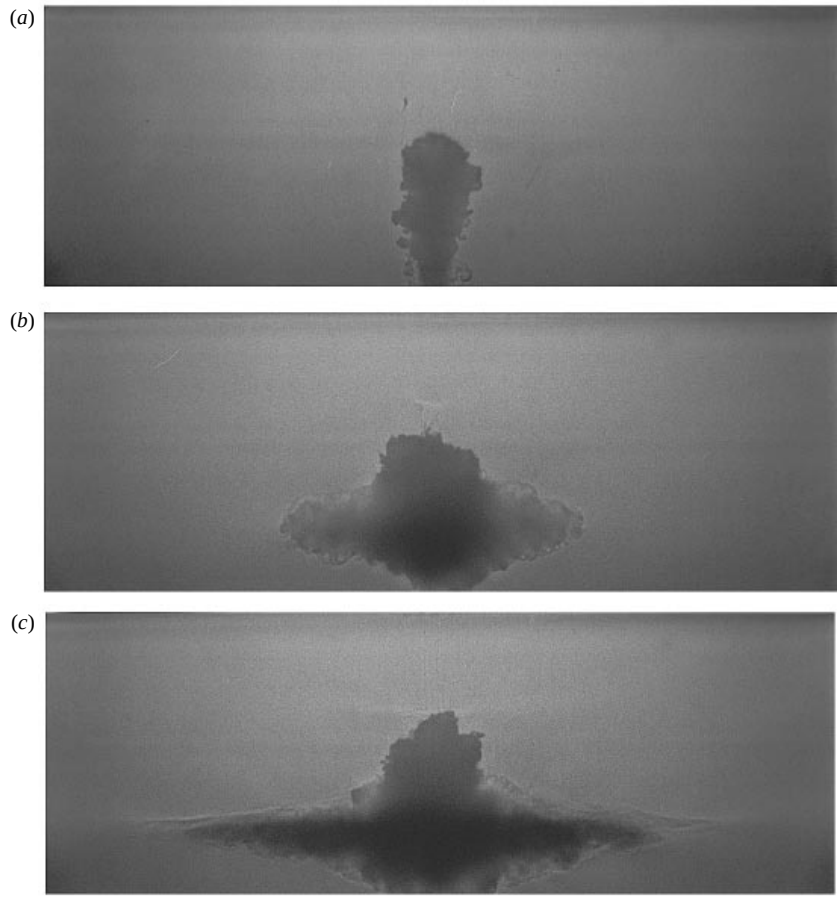

FIGURE 1. Photographs of an axisymmetric fountain where the density of the input fluid is equal to that at the base of the environment, the input volume flux is $4.5\times10^{-5}\,\mathrm{m^3\,s^{-1}}$ and the density gradient is $0.3\,\mathrm{kg\,m^{-4}}$. (*a*) The flow rises initially as a jet, entraining surrounding fluid ($t = 3\,\mathrm{s}$), until it reaches an initial height. (*b*) After reaching the initial height, the falling fluid intrudes into the environment ($t = 10\,\mathrm{s}$). (*c*) A layer forms as fluid continues to intrude at the same height ($t = 30\,\mathrm{s}$).

first outline the qualitative behaviour of axisymmetric and line fountains in a stratified fluid. We then present our quantitative results for axisymmetric sources in § 3 and for line sources in § 4. In § 5 we apply our results to two physical problems: the replenishment of magma chambers and the heating or cooling of a room. Finally, the main conclusions are summarized in § 6.

2. Qualitative observations

Fountains are produced in the laboratory by injecting dense fluid upwards through a nozzle placed on the base of a tank containing a stably stratified fluid which at all heights has a density less than or equal to the source fluid. The environmental fluid is entrained into the initial upflow, increasing the fountain radius (figure 1 *a*), and decreasing the source fluid density. The momentum of the rising fluid is reduced by the opposing buoyancy force until the flow first comes to rest at an initial height above the source. The downflow which forms after this point continues to mix with the environment while also interacting turbulently with the upflow. This interaction

restricts the rise of further fluid and therefore reduces the initial fountain height to a final value about which there are random fluctuations on the scale of 5–10% of the fountain height.

The final density of the downflow depends on the strength of the ambient stratification. In a homogeneous environment the falling fluid always remains denser than the ambient, so the flow must spread along the base of the tank. However, when the density of the source fluid is the same as that at the base of a gradient, any entrainment of ambient fluid must reduce the density of the downflow to equal that in the environment at some intermediate height. At this point, the flow still has some downward momentum, so a small overshoot is observed before it intrudes into the environment (figure 1 *b*). The thickness of this outflow is comparable to the spreading height near the fountain axis but quickly becomes thinner with increasing radial distance (figure 1 *c*). In all cases in which the source fluid has a negative buoyancy at the base of a tank of stably stratified fluid, the fountain flow lies between these two limits of behaviour.

Qualitatively similar behaviour is observed in the flow from a line source. Just after starting the flow, the injected fluid rises through the environment (figure 2 *a*) until first coming to rest at an initial height. In this case, however, the initial height is not significantly reduced by the interaction between the upflow and subsequent downflow. Depending on the strength of the stratification, the falling fluid may again either spread along the base or intrude into the environment at a height of neutral buoyancy (figure 2 *b*). The thickness of this intruding layer once more decreases with increasing distance from the axis of the flow. The profile of a line fountain oscillates randomly between an asymmetric (figure 2 *b*) and symmetric (figure 2 *c*) profile. During the intervals in which the downflow is deflected to one side of the upflow, a corresponding decrease in the final fountain height is observed. These additional instabilities were also seen in a homogeneous environment (Baines *et al.* 1990), although the fluctuations in our case are reduced by the ambient density stratification, resulting in a more stable fountain.

3. Axisymmetric fountains

The investigation of axisymmetric fountains proceeds as follows. We begin by describing the experimental apparatus and methods in § 3.1. In § 3.2 we study the fountains produced in the simple case where the source fluid and the ambient fluid at the base of the tank have the same density, resulting in a zero buoyancy flux at the source. First, in § 3.2.1, we compare the experimental data for the initial, final and spreading heights to the length scale obtained from dimensional analysis. In § 3.2.2, we use the entrainment equations to develop a numerical model to describe the flow. These numerical results are then compared to the experimental data to estimate an effective value of the entrainment coefficient. In § 3.3 we present the experimental data, dimensional arguments and numerical results for the general case in which the density of the source fluid is greater than that of the ambient at the base of the tank.

3.1. *Experimental methods*

The experiments were carried out in an acrylic tank 40 cm × 40 cm in cross-section and 80 cm deep, which was filled to a depth of approximately 25 cm. The ambient linear density gradient was established with NaCl solutions using the double bucket method (Oster 1965). The fluid densities were measured by refractometry to within 0.1%, giving a relative error in the density gradient of approximately 1%.

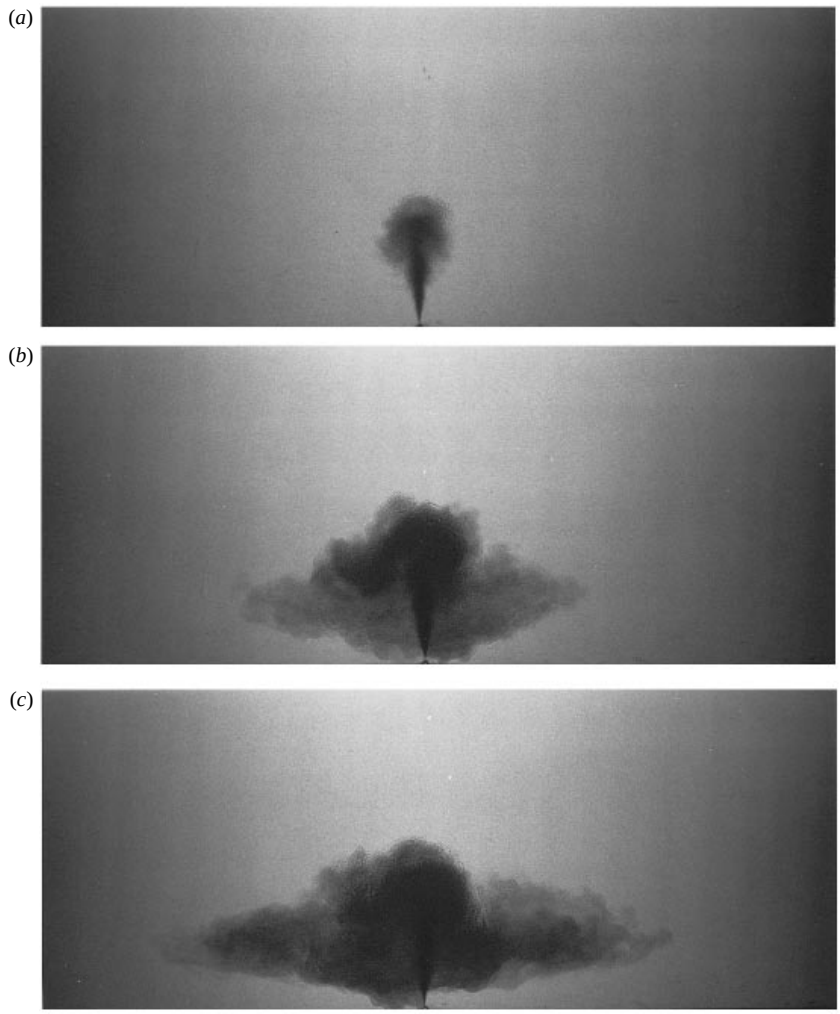

FIGURE 2. Photographs of a line fountain where the density of the input fluid equals that at the base of the tank, the input volume flux per unit length is 8.8×10^{-5} m^2 s^{-1} and the density gradient is 0.06 kg m^{-4}. (*a*) The fluid rises initially as a line jet ($t = 10$ s) before it reaches an initial height. (*b*) After the fluid starts to intrude into the environment, the fountain profile may become asymmetric ($t = 30$ s). When this occurs, the fountain height decreases. (*c*) The fountain fluctuates randomly between an asymmetric and a symmetric profile ($t = 50$ s).

The source fluid was placed in a 20 l bucket which was raised 1.5 m higher than the main tank. The flow rate resulting from this gravitational head was adjusted with a valve and measured with a flow meter to an accuracy of 1–4%. The source fluid was injected upwards from the base of the tank through a tube with an 8.8 mm inner diameter.

The flows were observed using the shadowgraph method and were recorded on video. This procedure allowed the fountain heights to be measured to within 0.5 cm (2–5% of the fountain height), and an average value of the fluctuating final height to be found over a period of time.

In preliminary experiments, the flow from the source was laminar for the first 2–3 cm, so wire crosshairs were introduced within the tube to induce turbulence. One

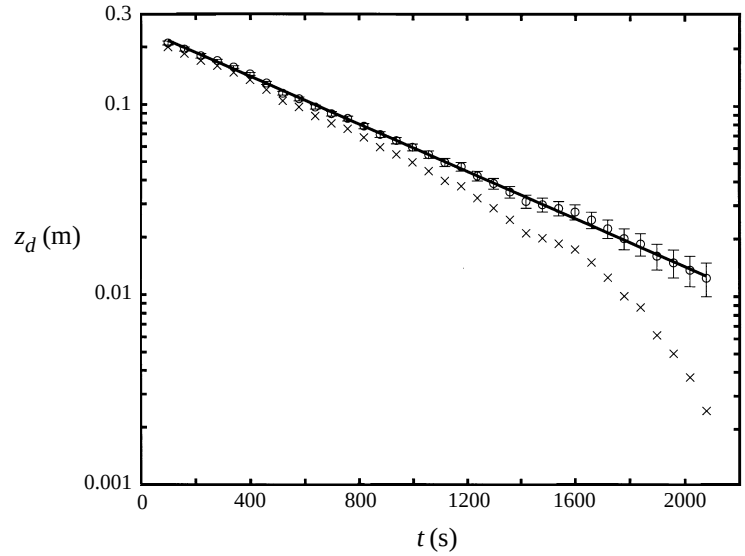

FIGURE 3. The position of the front formed by a jet in a homogeneous environment. The crosses represent heights measured above the base of the tank, while the circles are the heights above the virtual point source which is located 1 cm below the base of the tank. The slope of the line then indicates that the effective source radius is $r_e = 4.16$ mm.

set of 0.5 mm diameter crosshairs was positioned 3 mm from the tube outlet and the second set aligned and placed 44 mm further along the tube. The effect of these crosshairs was determined quantitatively by performing an experiment with a weakly buoyant jet in a homogeneous environment (Baines *et al.* 1990). The injected source fluid rose until it impinged on the free surface before spreading laterally towards the tank walls. The horizontal boundary, or *front*, which separated this fluid layer from the ambient then descended through the environment as more fluid from below it was entrained into the upflow and added to the layer above. The motion of this boundary is quantified by considering the conservation of volume flux at the height of the front:

$$\frac{\mathrm{d}}{\mathrm{dt}}(Az_d) = -Q_j(z_d), \tag{1}$$

where A is the cross-sectional area of the tank, z_d is the height of the front above the virtual point source, $Q_j = 2\alpha(\pi M_o)^{1/2} z_d$ (Rodi 1982) is the volume flux in the jet assuming a top-hat velocity profile, and α is the entrainment coefficient. The momentum flux at the source, $\rho_i M_o$, is not measured directly, but is related to the volume flux at the source, Q_o, by $M_o = Q_o^2/(\pi r_e^2)$, where ρ_i is the density of the source fluid and r_e is the effective source radius. For fully turbulent flow, r_e is equal to the measured source radius, r_o, while in laminar flow, $r_e = \sqrt{3} r_o/2$. Integrating (1) gives

$$z_d = z_H \exp\left(-\frac{2\alpha Q_o}{A r_e} t\right), \tag{2}$$

where z_H is the height at which the fluid initially spreads out along the free surface and $\alpha = 0.076$ (Rodi 1982). To determine the position of the virtual point source, z_v, its assumed location was varied until, when $z_v = 1.0 \pm 0.2$ cm below the base of the tank, the plot of $\ln(z_d)$ against time resulted in a straight line (figure 3). Then, from the slope of this line, the effective source radius was found to be $r_e = 4.16 \pm 0.23$ mm.

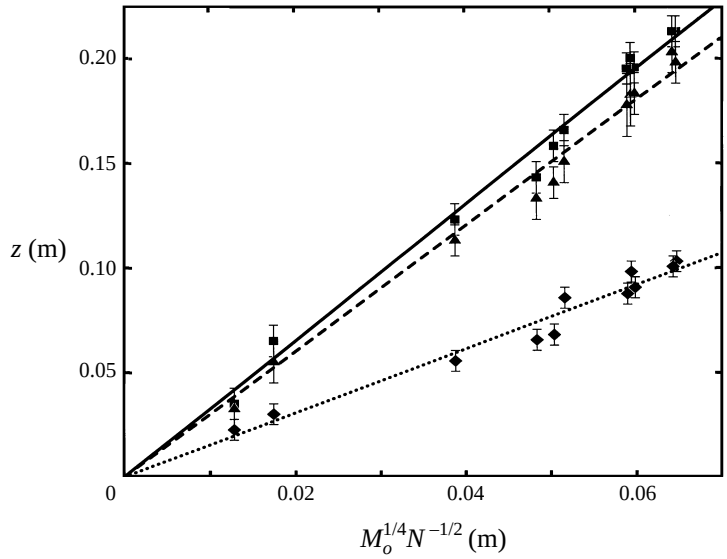

FIGURE 4. The initial (■), final (▲) and spreading (◆) heights of an axisymmetric fountain plotted against the length scale for the flow with a zero buoyancy flux at the source.

We therefore conclude that the crosshairs have significantly increased the turbulence at the source.

Morton (1959 *a*) showed that, even with a density difference between the source and environmental fluid, the lower part of the flow arising from a source of momentum is not significantly different from that of a jet. Hence, for our fountain experiments in which the flow in the region between the virtual and actual sources remains jet-like, the values of r_e and z_v can be assumed to remain invariant.

3.2. *Zero buoyancy flux at the source*

In the simple case when the density of the source fluid is equal to the ambient at the base of the tank, the flow depends only on two parameters: the momentum flux at the source, $\rho_i M_o$, and the buoyancy frequency, which is defined by $N = \left(-(g/\rho_o)(\mathrm{d}\rho/\mathrm{d}z)\right)^{1/2}$, where g is the gravitational acceleration, ρ is the environmental density, ρ_o is the density at the base of the tank and z is the height above the base. Dimensional arguments indicate that the only length scale that can be obtained from a combination of these parameters is $M_o^{1/4}N^{-1/2}$ (Fischer *et al.* 1979). The initial fountain height, z_i, the final height, z_f, and the spreading height, z_s, must all therefore take the form

$$z = CM_o^{1/4}N^{-1/2}, \tag{3}$$

where C is an unknown constant.

3.2.1. *Experimental results*

Eleven experiments were performed to determine the values of the constants C_i, C_f and C_s for the initial, final and spreading heights respectively. The volume flux at the source Q_o was in the range $(2\text{–}34)\times10^{-6}$ m^3 s^{-1} and the buoyancy frequency N was in the range 0.9–1.8 s^{-1}.

The experimental results for the three heights are plotted against $M_o^{1/4}N^{-1/2}$ in figure 4. Straight lines constrained to pass through the origin were fitted by a

least-squares method through the data points, confirming the linear relationship in (3). From the slope of these lines the constants are found to within two standard deviations to be $C_i = 3.25 \pm 0.17$, $C_f = 3.00 \pm 0.23$ and $C_s = 1.53 \pm 0.10$. The ratio of the initial to final fountain height is on average 1.08, a value much lower than the ratio of 1.43 observed in a homogeneous environment (Turner 1966). The reason for the smaller ratio is that when intermediate intrusion occurs, the interaction between the up- and downflows takes place over a shorter distance, leading to less reduction of the initial height.

3.2.2. *A numerical model*

The initial fountain height can also be predicted from a numerical solution of the entrainment equations, which describe the conservation of volume, momentum and buoyancy in the flow. In a stratified environment, 'top-hat' profiles, in which the parameters are constant throughout the area of the fountain and zero outside, are used to represent the average values in the flow (Morton 1959*b*). The entrainment equations are therefore

$$\frac{\mathrm{d}}{\mathrm{d}z}(b^2\omega) = 2\alpha b\omega, \quad \frac{\mathrm{d}}{\mathrm{d}z}(b^2\omega^2) = b^2\Delta, \quad \frac{\mathrm{d}}{\mathrm{d}z}(b^2\omega\Delta) = -b^2\omega N^2, \tag{4}$$

where z is the height above the source, b is the fountain radius, ω is the axial velocity of source fluid, $\Delta = (g/\rho_o)(\rho_f - \rho)$ is the effective gravitational acceleration with ρ_f the density of the fountain fluid, and α is the entrainment coefficient (Turner 1973, p. 171). By defining the quantities $Q = b^2\omega$, $M = b^2\omega^2$ and $F = b^2\omega\Delta$, equations (4) become

$$\frac{\mathrm{d}Q}{\mathrm{d}z} = 2\alpha M^{1/2}, \quad \frac{\mathrm{d}M^2}{\mathrm{d}z} = 2FQ, \quad \frac{\mathrm{d}F}{\mathrm{d}z} = -N^2Q. \tag{5}$$

While the measured buoyancy flux at the actual source is equal to zero, there is a finite but unknown buoyancy flux at the virtual source. The integration of (5) is therefore started at a height $z = z_v$ with the source conditions given by $Q = Q_o/\pi$, $M = M_o/\pi$ and $F = 0$ for the volume, momentum and buoyancy fluxes respectively.

Equations (5) were solved numerically over the experimental range of values of Q_o and N^2 using a routine based on a fourth-order Runge–Kutta scheme. For each value of the length scale $M_o^{1/4}N^{-1/2}$, the point at which the momentum flux first equals zero gives a value of the initial height. This integration was repeated for various values of α to obtain the best agreement between the experimental and numerical values for the initial fountain height (figure 5). An effective value of α for our fountain is thus found to be $\alpha = 0.085 \pm 0.010$, which is not significantly different from the jet entrainment coefficient of $\alpha_j = 0.076 \pm 0.004$ (Fischer *et al.* 1979).

The entrainment equations do not describe the mixing between the upflow and downflow or the additional entrainment of ambient fluid into the downflow that occurs after the fountain has reversed direction, so it is not possible to obtain an exact solution for the spreading height. However, the buoyancy, and thus the density of the fountain fluid at the initial height, before the downflow has formed, can be found from the solution of (5). The height in the environment where fluid with this density would intrude represents an initial estimate of the spreading height.

Included in figure 5 is the estimate of the spreading height which was calculated using $\alpha = 0.085$. The agreement between this numerical estimate and the experimental data is surprisingly good, given that the simple numerical model neglects two significant effects. Firstly, it does not include the interaction between the upflow and downflow which will tend to reduce the fountain height from its initial value, causing

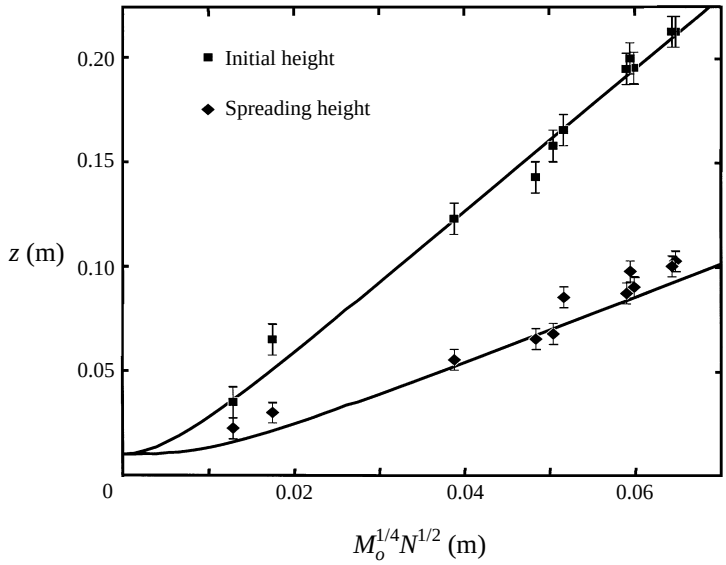

FIGURE 5. Comparison between experimental and numerical results for the initial and spreading heights of an axisymmetric fountain with a zero buoyancy flux at the source.

the falling fluid to intrude at a lower level. In this respect, the model overestimates the spreading height. Secondly, it does not allow the density of the falling fountain fluid to decrease as a result of the additional mixing with the lighter environment. The omission of this effect therefore results in an underestimate of the spreading height. From the reasonable agreement between the experimental and numerical results, it appears that these two neglected effects largely offset each other.

3.3. *Non-zero buoyancy flux at the source*

The fountain behaviour in this general case depends on M_o, N and the buoyancy flux at the source, $\rho_i F_o = \rho_i \Delta_o Q_o$, where $\Delta_o = (g/\rho_o)(\rho_i - \rho_o)$. In this case, there is no unique length scale, so we have chosen to write an expression for the three heights in terms of the length scale for a homogeneous environment (Turner 1966):

$$z = f(\sigma) M_o^{3/4} F_o^{-1/2}. \tag{6}$$

The dimensionless parameter, σ, has previously been introduced by Fischer *et al.* (1979) and is defined by

$$\sigma = \frac{M_o^2 N^2}{F_o^2}. \tag{7}$$

The effect of the density gradient is therefore included in the unknown $f(\sigma)$, which is different for the three heights.

An understanding of the physical significance of σ can be gained by writing it in an alternative form,

$$\sigma = \frac{-r_e Fr \, \mathrm{d}\rho/\mathrm{d}z}{(\rho_i - \rho_o)/Fr}, \tag{8}$$

where the Froude number is defined by $Fr = \omega_o/(r_e \Delta_o)^{1/2}$, and ω_o is the initial velocity of the source fluid. In a homogeneous environment, both the dimensionless fountain height, z_f/r_e, and the volume of environmental fluid entrained into the fountain

depend linearly on Fr (Baines *et al.* 1990). Hence, the numerator in (8) is a measure of the ambient density variation over the fountain height, while the denominator is a measure of the final density difference between the fountain and ambient fluids. The parameter σ therefore quantifies the relative magnitudes of the two buoyancy effects that control the behaviour of the fountain.

3.3.1. *Experimental results*

To determine the form of $f(\sigma)$ for the three heights, twenty four experiments were performed using values of Q_o in the range (11–45) $\times 10^{-6}\,\mathrm{m}^3\,\mathrm{s}^{-1}$, Δ_o between 0.01–0.53 $\mathrm{m\,s}^{-2}$ and N in the range 0.3 to 1.8 s^{-1}. The dimensionless initial and final heights are plotted with the known asymptotic limits of $f(\sigma)$ in figures 6(*a*) and 6(*b*) respectively. The experimental data approaches to within 5% of the large-σ limit at $\sigma \approx$ 20–40. The difference between the experimental data and the known homogeneous limit falls to 5% at $\sigma \approx$ 0.1–0.5.

As previously discussed for the case of a zero buoyancy flux at the source, the ratio of the initial to the final fountain height is less than that observed in a homogeneous fluid. Figure 6(*c*) shows explicitly how this ratio decreases as the dimensionless spreading height, $M_o^{-3/4}F_o^{1/2}z_s$, increases. This effect is due to the increasing spreading height reducing the distance over which the up- and downflows interact, as discussed in § 3.2.1.

The effect of the changing ambient density gradient on the dimensionless spreading height is shown in figure 7. In a homogeneous environment the intrusion occurs along the base of the tank, and in a stratified environment the spreading height must again approach zero as $\sigma \to \infty$. Hence there is a value of the density gradient at $\sigma_m \approx$ 40–60 which gives a maximum in the dimensionless spreading height. From figures 6(*a*) and 6(*b*), we see that this value of σ is close to the point at which the asymptotic limit for large σ becomes valid.

To determine the value of σ_c, the critical point at which the spreading height first rises from the base of the tank, $M_o^2N^2$ is plotted against F_o^2 (figure 8). The data corresponding to an intermediate spreading height are represented by open circles while filled circles indicate basal spreading. The slope of the line which separates these two regimes of behaviour is equal to σ_c, giving $\sigma_c = 5.0 \pm 0.1$.

3.3.2. *A numerical solution*

As in § 3.2.2, the entrainment equations were solved for a range of values of Q_o, Δ_o and N^2, with the integration of (5) starting at $z = z_v$ and the source conditions given by $Q = Q_o/\pi$, $M = M_o/\pi$ and $F = F_o/\pi$ for the fluxes of volume, momentum and buoyancy respectively.

Figure 9 shows both the experimental results for the initial height and the numerical solution of (5) calculated using $\alpha = 0.085$, the value found for the simple case of a zero buoyancy flux at the source. This numerical solution for the initial height is similar to that obtained by Morton (1959*a*, figure 4) for the flow from a point source, although it is plotted in a different form here. Also shown in figure 9 is the estimate of the spreading height based on the simple numerical model developed in § 3.2.2, and calculated using $\alpha = 0.085$. Numerical estimates of σ_c and σ_m are found to be $\sigma_c = 4.0$ and $\sigma_m = 30$, in comparison to the experimental results of $\sigma_c = 5.0$ and $\sigma_m =$ 40–60.

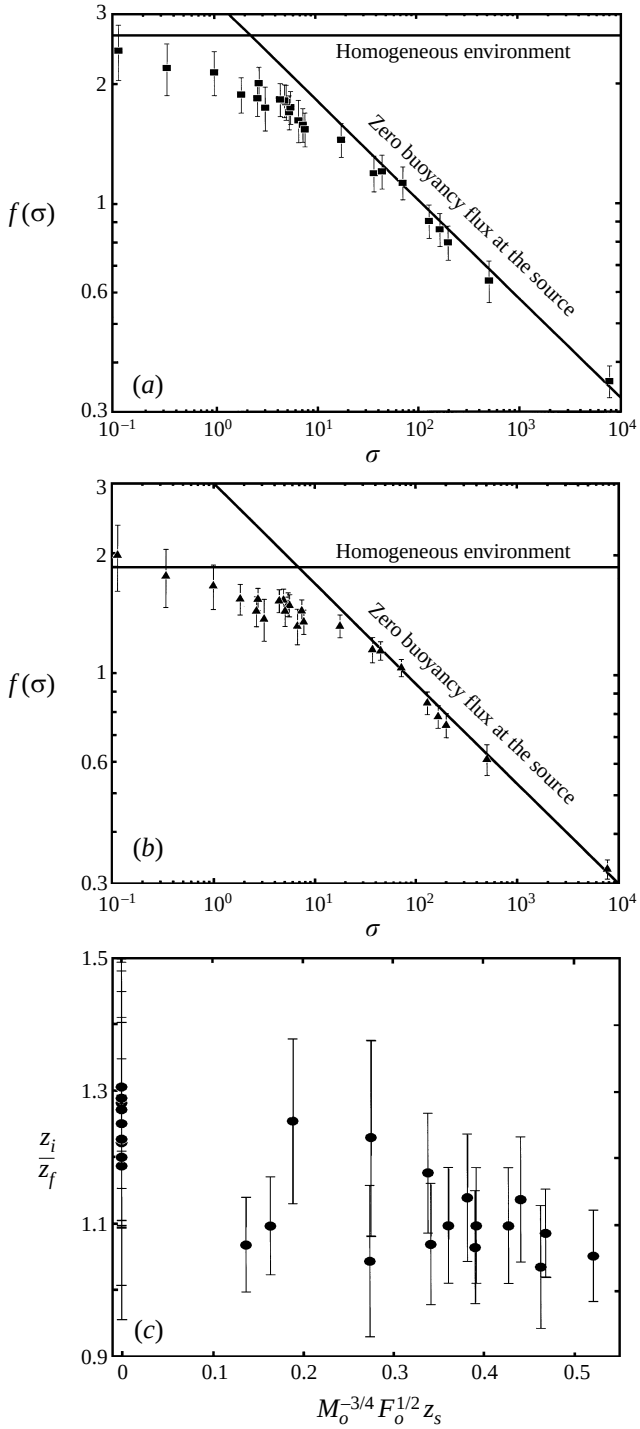

FIGURE 6. Dimensionless heights of an axisymmetric fountain showing the asymptotic results. (*a*) Initial height: as $\sigma \to 0$, $f(\sigma) \to 2.65$ (Turner 1966), and as $\sigma \to \infty$, $f(\sigma) = 3.25\sigma^{-1/4}$. (*b*) Final height: as $\sigma \to 0$, $f(\sigma) \to 1.85$ (Turner 1966), and as $\sigma \to \infty$, $f(\sigma) = 3.00\sigma^{-1/4}$. (*c*) Ratio of the initial to final height of an axisymmetric fountain showing the decrease in the ratio as the spreading height increases.

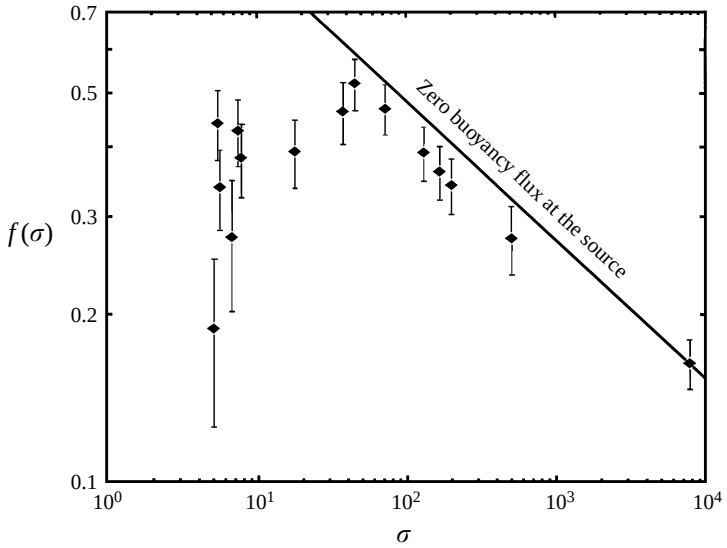

FIGURE 7. Dimensionless spreading height of an axisymmetric fountain as a function of σ showing the transition to the asymptotic behaviour for large σ, where $f(\sigma) = 1.53\sigma^{-1/4}$.

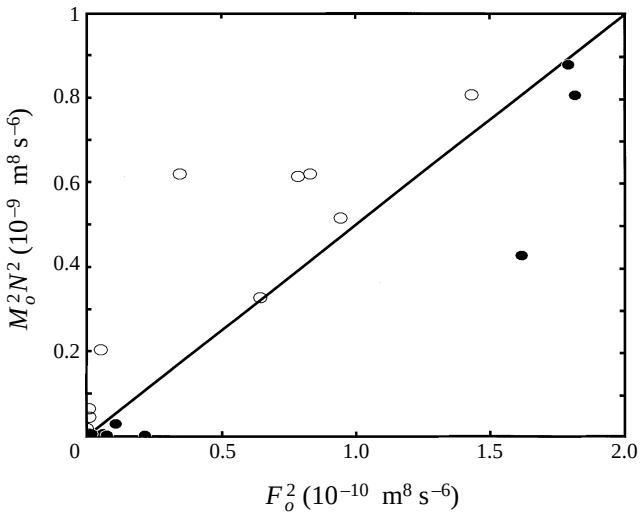

FIGURE 8. The data for experiments with an intermediate spreading height (○) and in which spreading occurs along the base (●) are separated by the plotted line which has a slope of 5.0.

4. Line fountains

4.1. *Experimental methods*

For an investigation of the turbulent fountains arising from a line source, we used the same tank and line source as were employed by Baines *et al.* (1990). The acrylic tank was 120 cm × 10 cm in cross-section and 60 cm deep, and was filled to a depth of approximately 35 cm. Two rolls of wire mesh were placed in the ends of the tank to act as damping screens. These were necessary to prevent the formation of a mixed layer in the environment as a result of the downward deflection of the spreading layer as it reached the tank walls (Baines *et al.* 1990). The line source was

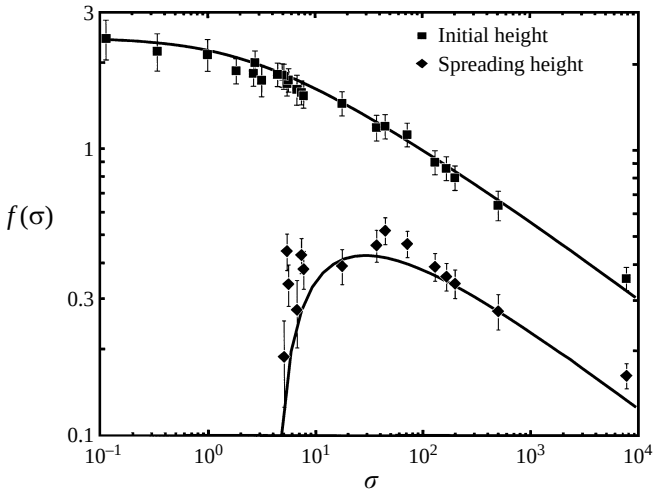

FIGURE 9. Comparison between experimental and numerical results for the initial and spreading heights of an axisymmetric fountain with a finite buoyancy flux at the source.

located centrally on the base of the tank, perpendicular to its length. This source was a circular pipe of 4 mm inner diameter with sixteen 0.5 mm holes drilled 5 mm apart along its length. The initial three-dimensional flow from the holes was observed experimentally to coalesce to two-dimensional flow within 3–4 cm of the source. The position of the virtual source and the equivalent slot width for this two-dimensional flow, b_o, was measured using the same method as was used by Baines *et al.* (1990) and described in § 3.1 for an axisymmetric fountain. Assuming a 'top-hat' velocity profile, the position of the descending front formed by a weakly buoyant line jet in a homogeneous environment is given by

$$z_d^{1/2} = H^{1/2} - \left(\frac{q_o^2 \alpha}{2 b_o L^2}\right)^{1/2} t, \tag{9}$$

where H is the height at which the fluid initially intrudes, $q_o = 2 b_o \omega_o$ is the volume flux per unit length of the source, $\alpha = 0.052$ (Rodi 1980) is the two-dimensional entrainment coefficient and L is the length of the tank (Baines *et al.* 1990). An experiment was performed to measure the height of the descending front, and a graph of $z_d^{1/2}$ against t was plotted. The graph was linear for $z > 4$ cm, indicating that for our experiments, the flow was two-dimensional for heights above 4 cm and that the virtual source was at the outlet of the holes. From the slope of the linear segment of the graph, the half-width of the source was calculated to be $b_o = 16.5 \pm 1.2$ μm. A similar value of $b_o = 16.4$ μm was obtained by Baines *et al.* (1990, p. 579) for the same source. It appears from their calculations that the value of α actually used was different from that reported ($\alpha = 0.106$).

4.2. *Zero buoyancy flux at the source*

In the special case of a zero buoyancy flux at the source, the initial, final and spreading heights of a line fountain must take the form

$$z = c\, m_o^{1/3} N^{-2/3}, \tag{10}$$

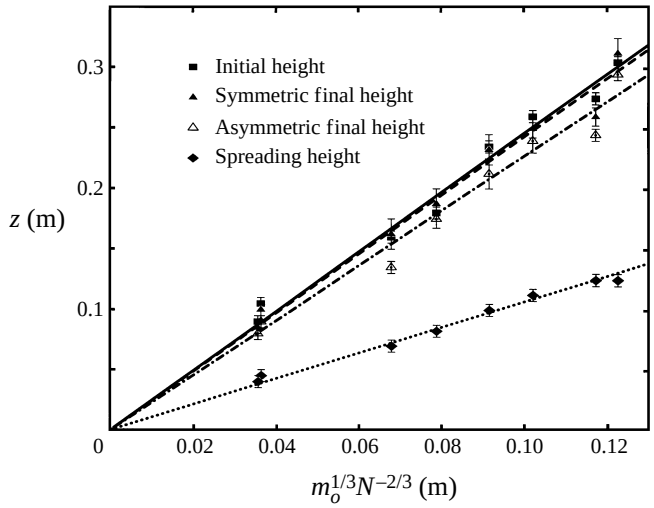

FIGURE 10. The initial, final symmetric, final asymmetric and spreading heights as a function of the length scale of a two-dimensional fountain with a zero buoyancy flux at the source.

where $\rho_i m_o$ is the momentum flux per unit length at the source, $m_o = q_o^2/2b_o$ and c is an unknown constant.

Eight experiments were performed with q_o in the range (3.2–10.1) $\times 10^{-5}\,\mathrm{m^2\,s^{-1}}$ and N in the range 0.4–1.4 $\mathrm{s^{-1}}$. Figure 10 shows the experimental measurements of the initial, final and spreading heights as a function of $m_o^{1/3}N^{-2/3}$. Two values of the final fountain height are plotted: those measured during the periods when the fountain profile was symmetric, z_{fs}, and asymmetric, z_{fa}. The straight lines fitted through the data points confirm the linear relationship in (10), and the constants are found within an error of two standard deviations to be $c_i = 2.46 \pm 0.08$, $c_{fs} = 2.43 \pm 0.20$, $c_{fa} = 2.27 \pm 0.20$ and $c_s = 1.07 \pm 0.05$ for the initial, final symmetric, final asymmetric and spreading heights, respectively.

In some experiments, the large fluctuations in the final symmetric height resulted in an average value that was greater than the initial height of the fountain. Hence, while most individual measurements indicate that the initial height is reduced by a small amount to the final value, the difference between c_i and c_{fs} is not statistically significant. This is in contrast to the corresponding difference of 30% observed in a homogeneous environment (Baines *et al.* 1990). Similarly, the 7% difference observed here between the symmetric and asymmetric final heights is much lower than the 20% difference that was measured in a homogeneous environment (Baines *et al.* 1990). These smaller height differences occur for the same reason as was discussed in § 3.3.1 for axisymmetric fountains, where the effect of intermediate intrusion reduces the distance over which the up- and downflows interact.

4.2.1. *Two-dimensional entrainment equations*

A numerical solution for the initial fountain height is obtained from the two-dimensional entrainment equations, which are

$$\frac{\mathrm{d}}{\mathrm{d}z}(b\omega) = \alpha\omega, \quad \frac{\mathrm{d}}{\mathrm{d}z}(b\omega^2) = b\Delta, \quad \frac{\mathrm{d}}{\mathrm{d}z}(b\omega\Delta) = -b\omega N^2, \tag{11}$$

where b is now the half-width of the fountain and the average values of ω and Δ are represented by top-hat profiles. In this case, the actual and virtual sources coincide,

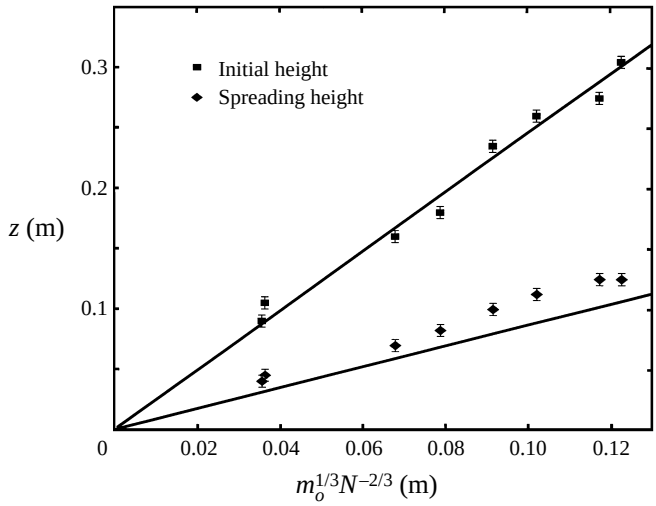

FIGURE 11. Comparison between experimental and numerical results for the initial and spreading heights of a two-dimensional fountain with a zero buoyancy flux at the source.

resulting in a unique length scale, so that we define the dimensionless quantities

$$\left.\begin{aligned} z = \alpha^{-1/3} m_o^{1/3} N^{-2/3} \tilde{z}, \quad b = \alpha^{2/3} m_o^{1/3} N^{-2/3} \tilde{b}, \\ \omega = \alpha^{-1/3} m_o^{1/3} N^{1/3} \tilde{\omega}, \quad \Delta = \alpha^{-1/3} m_o^{1/3} N^{4/3} \tilde{\Delta}. \end{aligned}\right\} \tag{12}$$

These allow the transformation to the dimensionless fluxes $\tilde{q} = \tilde{b}\tilde{\omega}$, $\tilde{m} = \tilde{b}\tilde{\omega}^2$ and $\tilde{f} = \tilde{b}\tilde{\omega}\tilde{\Delta}$, which then reduce (11) to

$$\frac{\mathrm{d}}{\mathrm{d}\tilde{z}}\tilde{q}^2 = 2\tilde{m}, \quad \frac{\mathrm{d}}{\mathrm{d}\tilde{z}}\tilde{m}^2 = 2\tilde{f}\tilde{q}, \quad \frac{\mathrm{d}}{\mathrm{d}\tilde{z}}\tilde{f} = -\tilde{q}. \tag{13}$$

The dimensionless fluxes per unit length at the source are specified by $\tilde{q}_o = 0$, $\tilde{m}_o = 1$ and $\tilde{f}_o = 0$, respectively, for the flow from a virtual line source.

The dimensionless initial height was found from a numerical solution of (13) to be $\tilde{z}_i = 1.06$. A comparison between the dimensionless forms of z defined in (10) and (12) leads to the relation $\alpha = (\tilde{z}_i/c_i)^3$. An effective value of α for our fountain is therefore found to be $\alpha = 0.080 \pm 0.008$, which again is not significantly different from the value of $\alpha_j = 0.074 \pm 0.004$ (Rodi 1982) for a jet.

The estimate of the spreading height obtained using the numerical model introduced in § 3.2.2 is shown in figure 11. In this case, the agreement between the experimental results and the numerical results, which were calculated using $\alpha = 0.080$, is not as good. For a line fountain, the initial height is approximately equal to the average final value, and so the numerical model only neglects the effects of the additional mixing between the downflow and the environment. This leads to a higher final density and thus lower spreading height than observed experimentally. From the magnitude of this difference between the experimental and numerical results, we estimate that the entrainment equations underestimate the total reduction in density of the source fluid by approximately 18%.

4.3. *Non-zero buoyancy flux at the source*

In this general case, the fountain heights take the form

$$z = f(\sigma^*) m_o f_o^{-2/3}, \tag{14}$$

where $\rho_i f_o = \rho_i \Delta_o q_o$ is the buoyancy flux per unit length at the source and the dimensionless parameter, σ^*, is defined by

$$\sigma^* = \frac{m_o^2 N^2}{f_o^2}. \tag{15}$$

To determine the form of $f(\sigma^*)$ for the three heights, twenty experiments were performed using values of q_o in the range (3.3–10.4) $\times 10^{-5}$ m^2 s^{-1}, Δ_o in the range 0.02–1.9 m s^{-2} and N in the range 0.17–1.4 s^{-1}. The dimensionless initial height is plotted with the known asymptotic limits in figure 12 (*a*). Figure 12 (*b*) shows the final heights measured when the fountain profile was both symmetric and asymmetric, along with the asymptotic limits for the symmetric final height. The experimental results approach to within 5% of the limit for large values of σ^* at $\sigma^* \approx 30$ for the initial height and at $\sigma^* \approx 100$ for the final symmetric height. For both heights, the deviation between the experimental results and the predicted homogeneous limit only falls to 5% at $\sigma^* \approx 0.4$.

The dimensionless spreading height is plotted in figure 12 (*c*), showing a rapid transition from a zero spreading height to a maximum in $f(\sigma^*)$ at $\sigma_m^* \approx 10$–20. Unlike the axisymmetric fountain, σ_m^* does not correspond to the value of σ^* at which the asymptotic limit for a zero buoyancy flux at the source becomes valid. A value of σ_c^* is found from the graph of $m_o^2 N^2$ against f_o^2 to be $\sigma_c^* = 6.0 \pm 0.1$ (figure 13).

4.3.1. *A numerical solution*

The dimensionless parameters for this general case are defined by

$$\left.\begin{aligned} z = \alpha^{-1/3} m_o f_o^{-2/3} \tilde{z}, \quad b = \alpha^{2/3} m_o f_o^{-2/3} \tilde{b}, \\ \omega = \alpha^{-1/3} f_o^{1/3} \tilde{\omega}, \quad \Delta = \alpha^{-1/3} m_o^{-1} f_o^{4/3} \tilde{\Delta}, \quad N^2 = m_o^{-2} f_o^2 \tilde{N}^2. \end{aligned}\right\} \tag{16}$$

Equation (11) then becomes

$$\frac{\mathrm{d}}{\mathrm{d}\tilde{z}}(\tilde{q}^2) = 2\tilde{m}, \quad \frac{\mathrm{d}}{\mathrm{d}\tilde{z}}(\tilde{m}^2) = 2\tilde{f}\tilde{q}, \quad \frac{\mathrm{d}}{\mathrm{d}\tilde{z}}(\tilde{f}) = -\tilde{N}^2 \tilde{q} \tag{17}$$

with the source conditions specified by $\tilde{q}_o = 0$, $\tilde{m}_o = 1$ and $\tilde{f}_o = -1$ for flow through a virtual line source.

The numerical results for the initial and spreading heights are shown in comparison with the experimental data in figure 14. The value of $\alpha = 0.080$ found for the case of a zero buoyancy flux at the source is used in these calculations, showing good agreement for the initial height over the wide range of values of σ^*. As before, the numerical estimate for the spreading height slightly underestimates the experimental results, although the critical points of $\sigma_c^* = 5.4$ and $\sigma_m^* = 32$ found from this estimate agree reasonably well with the experimental values of $\sigma_c^* = 6.00$ and $\sigma_m^* \approx 10$–20.

5. Applications

We now present two quantitative examples of how the results of this study can be applied to physical problems.

5.1. *The heating or cooling of a room*

In a reverse-cycle air conditioning system, axisymmetric turbulent fountains arise when hot air is forced downwards through the ceiling into a cold room, or when cold air is forced upwards through the floor into a hot room. Often it is preferable

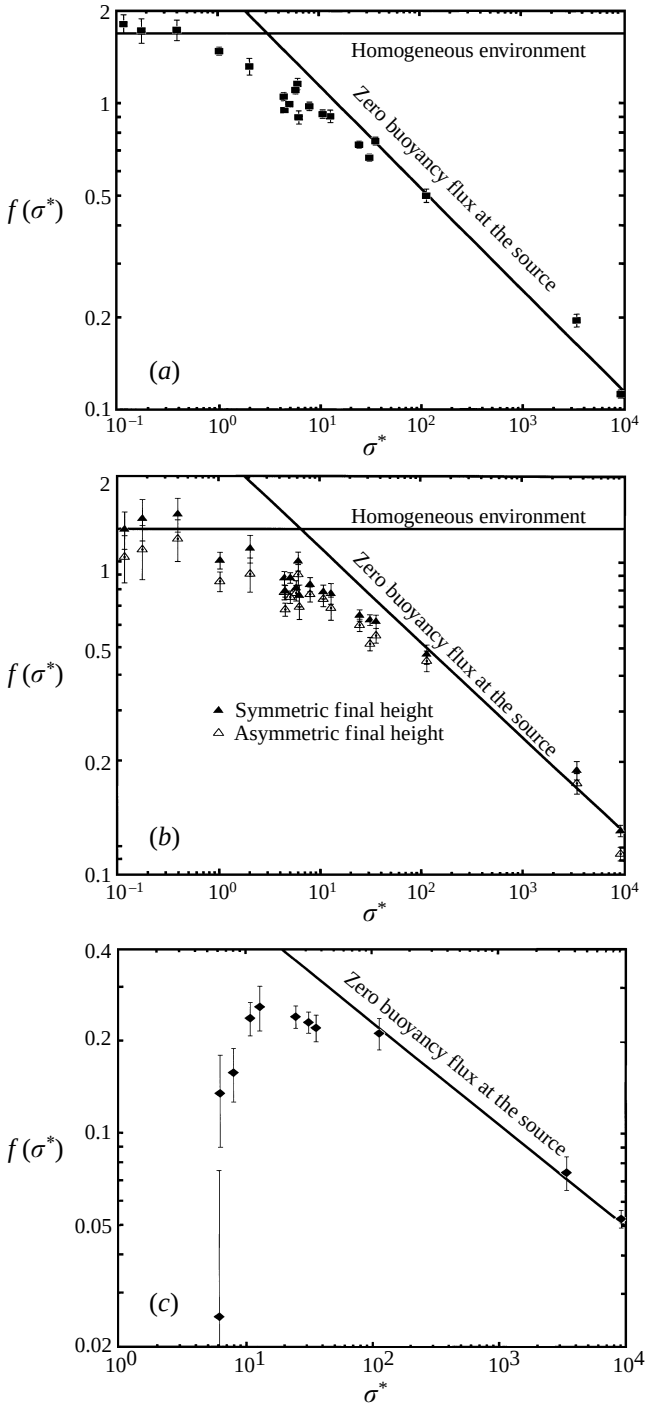

FIGURE 12. Dimensionless heights of a two-dimensional fountain with the asymptotic results. (*a*) Initial height: as $\sigma^* \to 0$, $f(\sigma^*) \to 1.69$ (Baines *et al.* 1990) and as $\sigma^* \to \infty$, $f(\sigma^*) = 2.46\sigma^{*-1/3}$. (*b*) Symmetric and asymmetric final height with the asymptotic results for the symmetric height: as $\sigma^* \to 0$, $f(\sigma^*) \to 1.3$ (Baines *et al.* 1990), and as $\sigma^* \to \infty$, $f(\sigma^*) = 2.43\ \sigma^{*-1/3}$. (*c*) Spreading height: as $\sigma^* \to \infty$, $f(\sigma^*) = 1.07\ \sigma^{*-1/3}$.

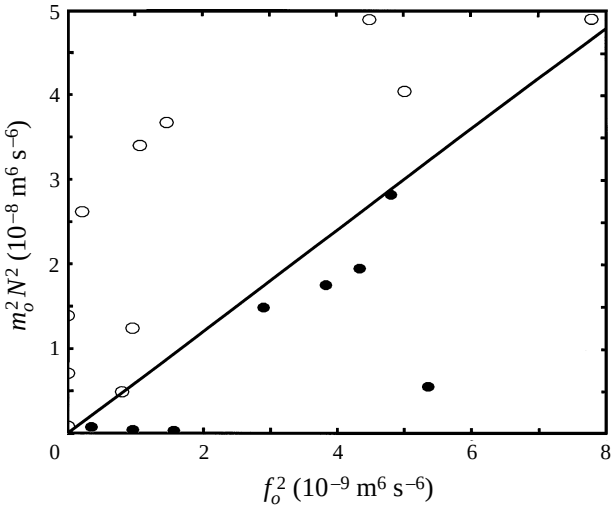

FIGURE 13. The data for experiments with an intermediate spreading height (○) and in which spreading occurs along the base (●) are separated by the plotted line which has a slope of 6.0.

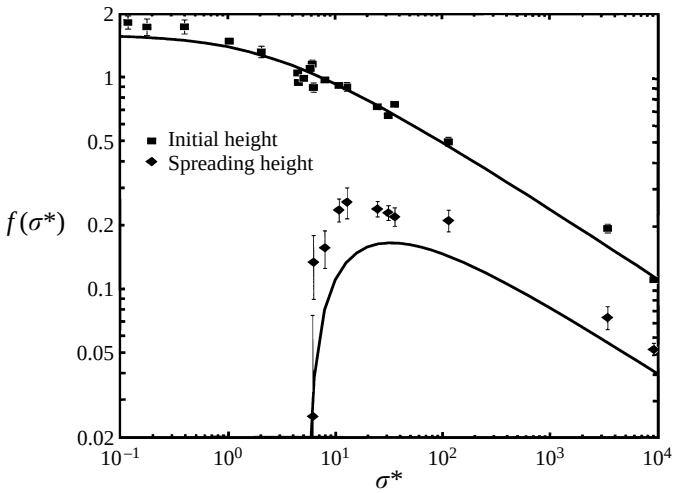

FIGURE 14. Comparison between numerical and experimental results for the initial and spreading heights of a two-dimensional fountain with a finite initial buoyancy flux. The value of $\alpha = 0.080$ was used in these numerical calculations.

to quickly heat or cool the lower region of the room. This most obviously occurs when cold air forms a fountain which spreads along the floor. The temperature of the injected air required to ensure basal spreading is calculated for typical environmental and input parameters.

Consider a room 4 m high and 5 m × 5 m in area, in which the ambient temperature of $T_f = 25\,^\circ$C at the floor increases with height at a rate of $1\,^\circ\mathrm{C\,m^{-1}}$. The buoyancy frequency is calculated using a thermal expansion coefficient of $\beta \approx \frac{1}{300}\mathrm{K^{-1}}$ to be $N = 0.18\ \mathrm{s^{-1}}$. Cold air could be forced upwards at a typical flow rate of $Q_o = 2\times10^{-2}\,\mathrm{m^3\,s^{-1}}$ through a vent with an area $\mathrm{A} = 0.01\ \mathrm{m^2}$. For the parameter σ to be

less than $\sigma_c = 5.0$, the temperature difference at the source must satisfy

$$\Delta T \geqslant \frac{Q_o N}{g\beta A \sigma_c^{1/2}}. \tag{18}$$

Using the parameters listed above, we find that the injected air will spread along the floor if $T_i \leqslant 20°\mathrm{C}$. The numerical solution for the initial height agreed well with the experimental results, and from this solution an estimate of the initial fountain height at $\sigma = 5.0$ is found to be $z_i = 2.4$ m above the floor. The final height is then estimated from figure 6(*c*) to be $z_f \approx z_i/1.25 = 1.9$ m.

When hot air is injected through the ceiling into a cold room, the region near the floor is not immediately affected by the fountain. A theory to describe the subsequent evolution of the room temperature with time is needed to determine the conditions required to optimize the heating of the room at floor level. However, the application of such a theory to this situation depends critically on the position of the return vent, as the removal of air also results in changes to the fountain's surroundings. The effects of a fountain in a confined stratified region will be investigated in a subsequent paper.

5.2. *The replenishment of magma chambers*

Hot magma that rises from deep within the Earth may form large chambers in the crust (Turner & Campbell 1986). These chambers, which can evolve from being homogeneous to having a density stratification, may then be replenished by the inflow of denser magma through a fissure at their base. If this new pulse of magma enters the chamber with sufficient upward momentum, a turbulent line fountain will result. The characteristics of these fountains can be predicted using our results from § 4.

We consider here fissure widths of $d = 1$ m, 3 m and 10 m, and a fixed input magma density of $\rho_i = 2650\,\mathrm{kg\,m^{-3}}$. We assume that the inflowing magma is forced through the fissure as a result of its buoyancy with respect to the surrounding wall rocks. If the flow is turbulent, the flow rate is given by

$$q_o = \left(\frac{g\Delta\rho}{f\rho_i}\right)^{1/2} d^{3/2}, \tag{19}$$

where g is the gravitational acceleration, $\Delta\rho$ is the average density difference between the input magma and the wall rocks of the fissure and f is a friction coefficient (Huppert & Sparks 1985). Probable values of $\Delta\rho = 300\,\mathrm{kg\,m^{-3}}$ and $f = 0.03$ are used here, although there is some uncertainty about the most appropriate values for these quantities, especially f, which is known to depend weakly on the flow parameters. To determine if the flow is turbulent, the Reynolds number, $Re = q_o\rho_i/\eta$, is calculated for each of the three fissure widths and for magma viscosities of $\eta = 1$ Pa s and 10 Pa s (table 1). In all cases, with the exception of the more viscous magma flowing through the smaller fissure, $Re > 2000$ indicating that the flow is turbulent. In this remaining case, turbulence may only just be developing.

To estimate realistic values of the environmental parameters, we consider the evolution of a magma chamber as the magma loses heat by conduction to the cold surrounding rocks. Initially, the magmas in the fissure and in the chamber have the same density and composition. As the temperature at the boundaries of the chamber decreases, olivine and pyroxene begin to crystallize. This crystallization decreases the density of the remaining magma, which buoyantly rises away from the boundaries and mixes turbulently with the overlying magma, leading to a homogenizing influence

	d=1 m	d=3 m	d=10 m
q_o ($m^2\ s^{-1}$)	6.1	32	192
Re ($\eta = 1$ Pa s)	1.6×10^4	8.5×10^4	5.1×10^5
Re ($\eta = 10$ Pa s)	1.6×10^3	8.5×10^3	5.1×10^4
Case I			
z_i (m)	81	146	476
z_f (m)	62	112	366
Case II			
z_i (m)	171	355	792
z_f (m)	168	350	782
z_s (m)	74	154	344
$\Delta\rho_e$ ($kg\ m^{-3}$)	5.1	10.6	23.7
Case III			
σ^*	2.0	6.1	19.9
z_i (m)	128	317	780
z_f (m)	≈ 111	≈ 261	≈ 672
z_s (m)	0	≈ 7	≈ 243
$\Delta\rho_e$ ($kg\ m^{-3}$)	2.6	6.3	15.6
ρ_c ($kg\ m^{-3}$)	2643	2640	2634

TABLE 1. Properties of the line fountains in magma chambers for three examples of different environmental density profiles

in the chamber (figure 15 *a*). As the temperature decreases further, plagioclase also begins to crystallize from the melt, increasing the density of the remaining magma. This dense fluid flows to the bottom of the chamber where it ponds, leading to a density stratification near the base (figure 15 *b*). The density profile therefore evolves from being completely homogeneous to having a stratified region overlayed by the homogeneous magma. In these examples we assume that in a chamber that is several kilometres in depth, only the lower 1 km is stratified.

We are now able to calculate the fountain heights and, where applicable, the ambient density variation over the initial height for three different examples of environmental density profiles (table 1).

Case I: Homogeneous environment The decrease in magma density as a result of the fractionation of olivine and pyroxene is generally small: a typical value of 30 $kg\,m^{-3}$ is used here (Campbell & Turner 1989). Hence, in the first stage of the evolution of the magma chamber, a fountain may be produced by the injection of the dense magma into a lighter homogeneous environment with a density of $\rho_o = 2620\ kg\,m^{-3}$. The initial and final heights of the fountain are obtained from the expressions determined by Baines *et al.* (1990) (see the caption to figure 12). As the fissure width increases so does the volume flux of the source magma, resulting in higher fountains. For the smallest fissure, in which turbulence may only just be developing, the fountain remains small compared to the height of the chamber, allowing little mixing between the magmas. For the wider fissures, the fountains can reach a height that allows significant interaction with the surrounding magma.

Case II: Zero buoyancy flux at the source The dense magma which ponds at the base of the chamber as a result of the crystallization of plagioclase can have a range of densities. In the later stages of fractionation, when the density at the base has increased to $\rho_b = \rho_i = 2650\ kg\,m^{-3}$, the fountain produced has a zero buoyancy flux at the source. The buoyancy frequency of the stratified region is calculated to be $N = 0.01\ s^{-1}$. The initial, symmetric final and spreading heights are calculated from (10)

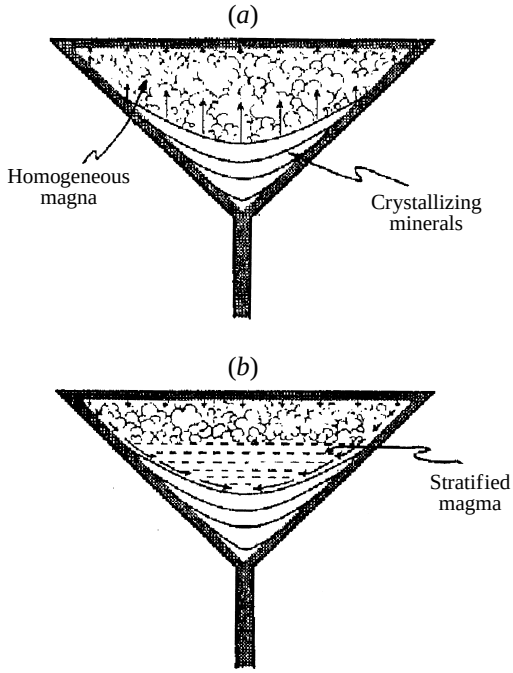

FIGURE 15. Evolution of a magma chamber as the temperature decreases (from Turner & Campbell 1986). (*a*) The fractionation of olivine and pyroxene releases light fluid which mixes turbulently through the chamber, resulting in a lighter homogeneous magma. (*b*) The dense fluid released as plagioclase crystallizes ponds at the base, establishing a density gradient. Dashed lines represent stratification, and swirls represent mixing. The vertical scale is exaggerated.

using the experimentally determined values of the constants from § 4.2. The initial height is a significant fraction of the depth of the stratified region, ranging from 171 m to 792 m as the fissure width increases. Further increase in the fissure width would result in a fountain that rises initially into the overlying homogeneous magma. The increase in the ambient density variation over the initial height, $\Delta\rho_e = z_i(\mathrm{d}\rho/\mathrm{d}z)$, is also calculated.

Case III: Non-zero buoyancy flux at the source Depending on the stage of plagioclase crystallization, ρ_b can increase from $\rho_b = 2620\ \mathrm{kg\,m^{-3}}$ (Case I) to $\rho_b = 2650\ \mathrm{kg\,m^{-3}}$ (Case II) before further increases result in the replenishing magma forming plumes rather than fountains. An illustrative example for the case of a finite buoyancy flux at the source uses $\rho_b = 2640\ \mathrm{kg\,m^{-3}}$ giving a buoyancy frequency of $N = 8.6 \times 10^{-3}\ \mathrm{s^{-1}}$. The three fissure widths give values of σ^* corresponding to the three regimes of behaviour: $\sigma^* < \sigma_c^*$, $\sigma^* \approx \sigma_c^*$ and $\sigma^* > \sigma_c^*$. The numerical results, which agreed well with the experiments, are used to estimate the initial fountain heights, while the final and spreading heights are found from the experimental data (figure 12). For the smallest fissure, the downflow spreads along the base of the chamber. As the width increases to 3 m, the conditions are close to those at which the spreading height first rises from the floor and the intrusion height is only 7 m. For the largest fissure, the fluid intrudes at a significant height above the floor. The initial heights which range from 128 m to 780 m again approach the top of the stratified region but do not extend beyond it for the fissure widths under consideration. We can also calculate the value of the density at the floor of the chamber

which corresponds to the critical conditions between intermediate and basal spreading. For this critical density ρ_c, $N^2 = -(g/\rho_c)(\rho_o - \rho_c)/H$ and $f_o = (g/\rho_c)(\rho_i - \rho_c)q_o$, giving

$$\sigma_c^* = \frac{m_o^2 \rho_c (\rho_c - \rho_o)}{H g q_o^2 (\rho_i - \rho_c)^2}. \tag{20}$$

Writing m_o in terms of q_o and rearranging (20) results in a quadratic expression for ρ_c, with the solution

$$\rho_c = \frac{2Hgd^2\sigma_c^*\rho_i - \rho_o q_o^2 - q_o(4Hgd^2\sigma_c^*\rho_i(\rho_i - \rho_o) + \rho_o^2 q_o^2)^{1/2}}{2(Hgd^2\sigma_c^* - q_o^2)}, \tag{21}$$

where $H = 1000$ m is the depth of the gradient.

6. Conclusions

We have presented an experimental and theoretical study of the behaviour of turbulent fountains in a stratified environment. In both axisymmetric and line fountains, there are two distinct regimes of behaviour. In the limit of a zero buoyancy flux at the source, the intrusion of the falling fluid occurs at an intermediate height in the environment. When the density difference between the input fluid and the environment is sufficiently large, spreading occurs along the base of the tank and the qualitative behaviour approaches that observed in a homogeneous environment. The conditions for which the experimental results approach these asymptotic limits were found in terms of a dimensionless parameter, σ, introduced previously by Fischer *et al.* (1979) and whose physical significance has been discussed. The transition from an intermediate spreading height to intrusion along the base occurred at a critical value of $\sigma_c = 5.0 \pm 0.1$ for an axisymmetric fountain and $\sigma_c^* = 6.0 \pm 0.1$ for a line fountain. The point at which the dimensional arguments for a zero buoyancy flux at the source become valid coincided approximately with a maximum in the spreading height at $\sigma_m \approx 40$–60 for the axisymmetric fountain. In line fountains, the maximum in the spreading height at $\sigma_m^* \approx 10$ occurred before the transition at $\sigma^* \approx 100$ to the asymptotic behaviour expected for large σ^*.

The solution of the entrainment equations for the initial fountain height was compared to the experimental results to give a value of $\alpha = 0.085 \pm 0.010$ for an axisymmetric fountain and $\alpha = 0.080 \pm 0.008$ for a line fountain. Using an approximate model and the experimentally determined values of α, the spreading height was also estimated from a solution of the entrainment equations. For the axisymmetric fountain, the numerical results agreed well with the experimental data, while the solution for the line fountain underestimated the experimental results.

We have shown how the results of this study can be applied quantitatively to physical problems. The effect of a density gradient on the spreading height of both cold air injected into a hot room and dense magma injected into a magma chamber has been calculated for typical environmental and source parameters. In most real situations where the environmental fluid is finite in extent, this initial fountain behaviour will evolve in time as the addition of source fluid alters the environment. These changes will be outlined in a subsequent paper.

We thank Tony Beasley, Derek Corrigan and Ross Wylde-Browne for their technical assistance with the experiments, and Stewart Turner and Ross Griffiths for their helpful comments on earlier drafts. The financial support of an Australian Research

Council Fellowship (for R. K.) and that of a Jaeger Scholarship (for L. B.) are gratefully acknowledged.

REFERENCES

Baines, W. D., Turner, J. S. & Campbell, I. H. 1990 Turbulent fountains in an open chamber. *J. Fluid Mech.* **212**, 557–592.

Campbell, I. H. & Turner, J. S. 1989 Fountains in magma chambers. *J. Petrol.* **30**, 885–923.

Fischer, H. B., List, E. J., Koh, R. C. Y., Imberger, J. & Brooks, N. H. 1979 *Mixing in Inland and Coastal Waters*. Academic.

Huppert, H. E. & Sparks, R. S. J. 1985 Komatiites I: Eruption and flow. *J. Petrol.* **26**, 694–725.

List, E. J. 1982 Turbulent jets and plumes. *Ann. Rev. Fluid Mech.* **14**, 189–212.

Morton, B. R. 1959*a* Forced plumes. *J. Fluid Mech.* **5**, 151–163.

Morton, B. R. 1959*b* The ascent of turbulent forced plumes in a calm atmosphere. *Intl J. Air Poll.* **1**, 184–197.

Morton, B. R., Taylor, G. I. & Turner, J. S. 1956 Turbulent gravitational convection from maintained and instantaneous sources. *Proc. R. Soc. Lond.* A **234**, 1–23.

Oster, G. 1965 Density gradients. *Sci. Am.* **213**, 70–76.

Rodi, W. 1982 *Turbulent Buoyant Jets and Plumes*. Pergamon.

Turner, J. S. 1966 Jets and plumes with negative or reversing buoyancy. *J. Fluid Mech.* **26**, 779–792.

Turner, J. S. 1973 *Buoyancy Effects in Fluids*. Cambridge University Press.

Turner, J. S. 1986 Turbulent entrainment: the development of the entrainment assumption, and its application to geophysical flows. *J. Fluid Mech.* **173**, 431–471.

Turner, J. S. & Campbell, I. H. 1986 Convection and mixing in magma chambers. *Earth Sci. Rev.* **23**, 255–352.